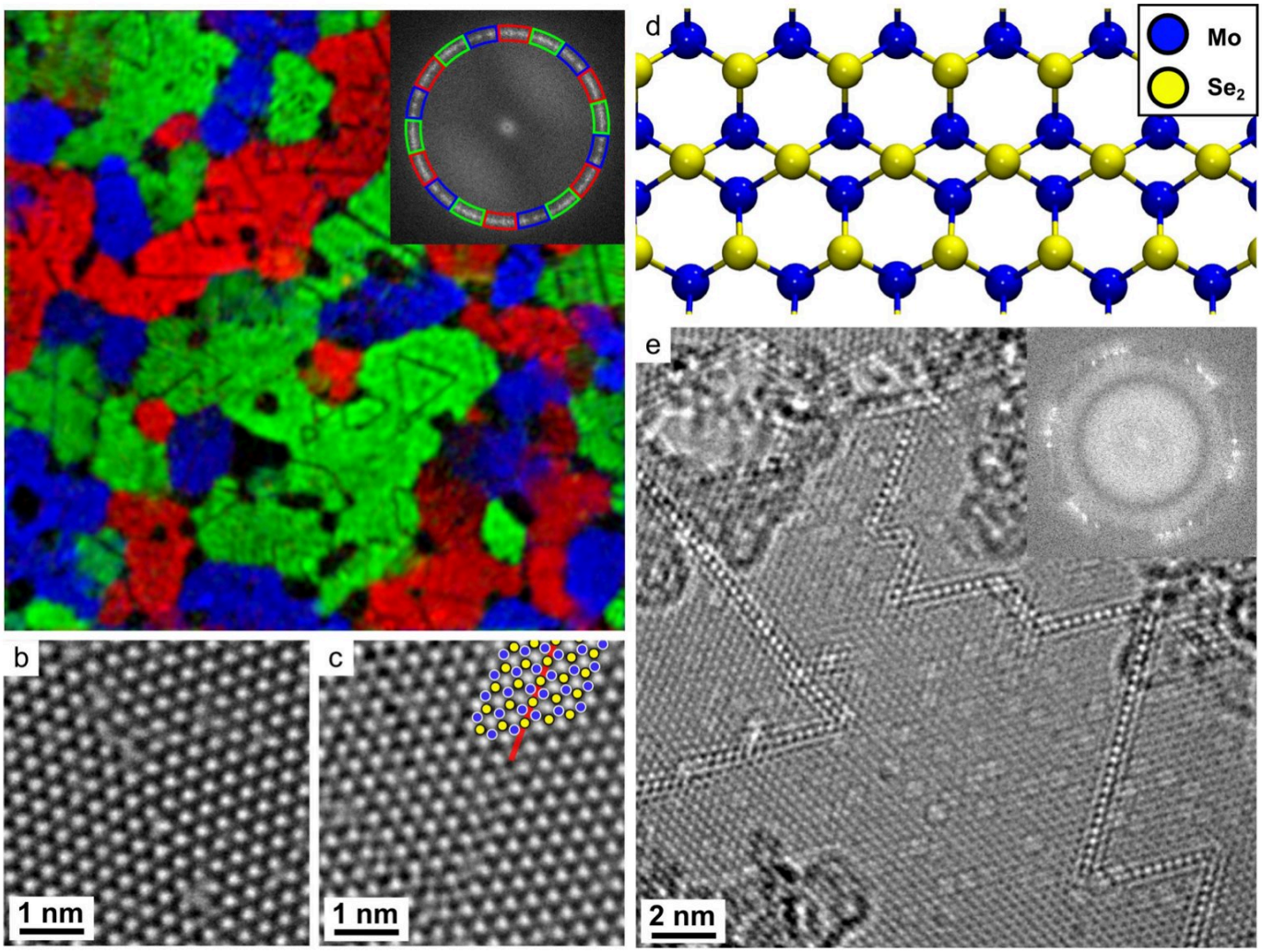

Fig. 1: Grains and mirror twin boundaries in MoSe2.

Se-Deficient 2D $MoSe_2$

March 11, 2015 · salve-project.de/newspress/microstructure-and-properties-of-Se-deficient-2D-MoSe2.html

March 11, 2015 – Single layers of $MoSe_2$ grown by molecular beam epitaxy with slightly too little selenium hide the deficit in a dense network of mirror twin boundaries inside their grains. Researchers from Ulm, Aalto University and EPFL Lausanne imaged them at 80 kV in Ulm on an FEI Titan with a CEOS C_s corrector and weighed the composition, $MoSe_{1.983}$, by counting the boundaries. DFT calculations show that the boundaries are the stable form of a selenium deficit, carry states along their length and block holes crossing them. Under the beam, new mirror twins formed, and at a very high selenium deficit the sheet turned into nanowires, which a 60 kV STEM study on a C_s-corrected Nion UltraSTEM 100 confirmed a year later.

Researchers from Ulm University, Aalto University in Finland and EPFL in Lausanne have looked at single layers of molybdenum diselenide ($MoSe_2$) that contain slightly too little selenium, and found out where the missing selenium goes: the layer hides the deficit in a dense network of line defects called mirror twin boundaries (MTBs)[1]. Changing the atomic composition of a material is one of the oldest ways to tune its properties. Perhaps the most famous example is the rich phase diagram of iron and iron carbide (Fe–Fe_3C), where the smallest changes in the carbon content have a large effect on the properties of processed iron[2]. For the new class of two-dimensional (2D) materials this approach is still largely unexplored.

Too little selenium

Transition metal dichalcogenides (TMDs) such as MoS_2 and $MoSe_2$ are technologically very interesting because of their electronic properties[3], and recently they have been produced as single layers by chemical vapour deposition[4]–[6]. The typical aim was to grow high-quality crystals at the perfect 1:2 composition, or alloys with three elements[7],[8], where the extra element re-

places atoms of the pure crystal either in the chalcogen[8],[9] or in the metal sublattice[10]. However, defects and dopant atoms can also be used to modify the properties of these materials[11],[12].

A recent study showed that the mobility of the charge carriers in 2D MoS_2 increases when the proportion of sulfur is reduced[13]. This is consistent with studies of bulk $MoSe_2$, where small deviations from the perfect composition change the charge carrier concentration[14] and the mass density[15]. In 2D, however, the range of stable compositions is narrow, since only some phases are layered at all[16]. If the selenium content of bulk $MoSe_2$ drops too far, the crystal crosses over to Mo_3Se_4, whose structure is three-dimensional. So what happens in a single layer that is short of selenium but stays two-dimensional?

Grains, boundaries and mirror twins

Ossi Lehtinen and his co-authors examined single layers of $MoSe_2$ grown by molecular beam epitaxy (MBE) by Andras Kis and co-workers at EPFL Lausanne. They imaged them in Ulm on an FEI Titan 80-300 (today Thermo Fisher Scientific), a transmission electron microscope whose imaging lens is corrected for spherical aberration by a CEOS corrector, operated at 80 kV. How the layers were grown and prepared is described in the box below. A year later, an independent study with a scanning transmission electron microscope (STEM), a C_s-corrected Nion UltraSTEM 100 at 60 kV, confirmed the nanowires found here, as the second validation box below shows.

Recipe: $MoSe_2$ layers from the MBE chamber

The $MoSe_2$ layers were grown at 450 °C in a customized MBE system on silicon chips covered with 270 nm of silicon dioxide. Selenium came from a Knudsen cell and molybdenum from an electron-beam source, with a Mo/Se flux ratio of about 1:30. Electron diffraction at grazing incidence (RHEED) followed the formation of the crystal during growth.

For the microscope, the films were coated with about 500 nm of PMMA, lifted off the substrate in hot potassium hydroxide solution, fished out of a water bath onto TEM grids, dried gently and freed of the PMMA with acetone. In the Titan, the extraction voltage of the field emission gun was lowered to 2 kV to reduce the energy spread of the beam, and the spherical aberration was corrected to less than 20 µm. The images were taken at negative defocus, so atoms appear dark.

The layers turned out to be a patchwork of very small grains, stitched together by tilt grain boundaries made of rows of dislocations (Fig. 1a, b), similar to what had been observed earlier in MoS_2[6] and graphene[17],[18]. Inside the grains, however, the team found a second kind of line defect: mirror twin boundaries (Fig. 1c, d). On both sides of such a boundary the lattice seems to have the same orientation, but the triangular $MoSe_2$ lattice is mirrored, so molybdenum and selenium sites swap places. The selenium sublattice continues across the boundary, while the molybdenum sublattice is interrupted, and the selenium atoms at the boundary bind to four molybdenum atoms instead of three. Only this one type of MTB was found. Such boundaries had also been used earlier to explain features in $MoSe_2$ films grown on a cleaved MoS_2 surface[19],[20].

Counting boundaries to weigh the composition

An MTB contains more molybdenum than the perfect lattice: one extra Mo atom per nanometre of boundary. Where MTBs are dense, the layer is therefore measurably short of selenium, and the length of all MTBs in an image tells how short. To map them quickly, the researchers used a trick: they set the focus so that the spatial frequency of the $MoSe_2$ lattice fell on a zero of the microscope's contrast transfer function. The regular lattice then all but vanishes from the image, while every break in it stands out, even under contamination (Fig. 1e).

In 18,700 nm^2 of imaged layer they measured 1730 nm of MTBs. This puts the composition inside the grains at $MoSe_{1.983}$, with an uncertainty of one in the last digit, and the mass density 0.32 % above that of perfect $MoSe_2$. The many single selenium vacancies visible in the images do not count: they were created by the electron beam during imaging, as shown further below.

Born during growth

Do the MTBs form when two grains grow into each other, or within a single growing grain? The statistics of the grain boundaries rule out the first: MTBs are far too frequent to come from randomly meeting grains, as the box below explains. They must therefore grow with the grain.

Background: why the mirror twins are not stitched-up grains

Two grains growing into each other form an MTB only if their lattices meet turned by close to 180°. The grains in the sample showed no preferred orientation, so all angles between neighbouring grains are equally likely. Earlier calculations[6] show that the boundary energy drops within about 10° of the ideal 180°. If grains meeting within this range turned into MTBs, one boundary in six would be an MTB.

The measurement found something quite different: 0.097 nm of tilt grain boundary and 0.093 nm of MTB per square nanometre, almost one to one. For that, grains would have to form MTBs at up to 30° away from 180°, but such large misfits are never seen at an MTB. In addition, the MTBs never lie where the leading Mo edges of two grains meet, so the grains grew in the direction of their Se edges. Star-like points from which several MTBs radiate look like the nuclei of grains, and closed MTB loops without any dislocation show that the domains were there from the start and were not cut later by the beam.

The calculations of the team explain why. Under molybdenum-rich growth conditions the formation energy of MTBs drops significantly, so more of them form during growth (Fig. 2b). Similar to what some of the authors had observed earlier in MoS_2[21],[22], lines of vacancies are more favourable than isolated ones, but in $MoSe_2$ such vacancy lines cost far more energy than

MTBs over the whole range of conditions. Also, selenium has a low sticking coefficient[23], which can produce a local selenium deficit even when more selenium than needed is supplied.

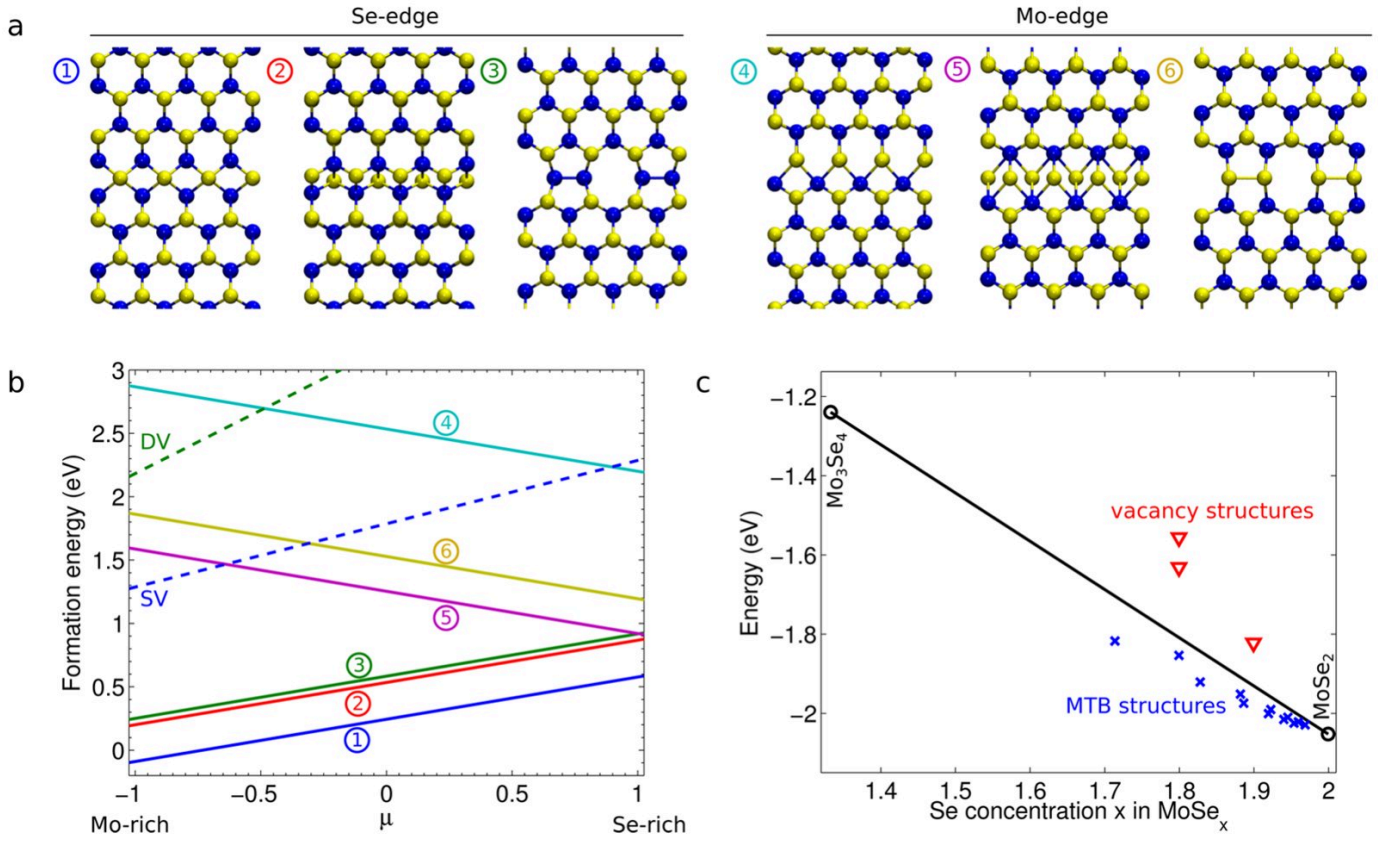

Fig. 2: Energies of MTBs and vacancy structures.

The preferred way to lack selenium

Density functional theory (DFT) calculations[24],[25] compared six possible MTB structures, built from facing Se edges or facing Mo edges (Fig. 2a). The structure seen in the experiment has the lowest energy, by a margin of 0.3 eV, and all boundaries built from Se edges beat those from Mo edges. The phase diagram of molybdenum and selenium between $MoSe_2$ and Mo_3Se_4 was so far unknown. Here the calculations are clear: a layer that takes up its selenium deficit with many MTBs has a lower energy than a mixture of $MoSe_2$ and Mo_3Se_4, while a layer full of vacancies is even higher in energy than the mixture (Fig. 2c). A selenium-deficient $MoSe_2$ layer in thermal equilibrium should therefore be full of mirror twin domains.

Channels along, barriers across

MTBs also change how charge moves through the layer. Along a straight boundary, extra electronic states could make it conduct better, while across it, holes are strongly held back. The box below shows the calculations, with the bands in the gap (Fig. 3), the states at the boundary (Fig. 4) and the transmission across it (Fig. 5).

Theory: electrons along and across a mirror twin boundary

The calculated band structure of a ribbon containing one MTB shows two bands localized at the boundary, which run through a wide energy range inside the band gap (Fig. 3a, b). Both come from the molybdenum atoms around the boundary (Fig. 4). Such states could give straight, periodic MTBs a higher conductivity along their length. In a real layer, however, electrons travelling along a boundary are scattered back at its turns and junctions, which may largely cancel the extra channels. Such a suppression of localized electronic states at the turns of grain boundaries had been observed only recently in polycrystalline graphene by the Swiss group that took part in this study[26]. Electrical measurements on the samples indeed showed no improvement, either for this reason or because of the many tilt grain boundaries.

Calculations of ballistic transport with nonequilibrium Green's functions (Fig. 5) show what happens across a boundary. Electrons in the conduction band pass with only moderately reduced probability, probably limited by resonant scattering on the localized states. For holes in the valence band, however, the transmission falls exponentially with decreasing energy. The reason is the electrostatic potential: calculated along the transport direction and averaged over the planes perpendicular to it, it bends downwards by about 0.1 eV over a wide region around the boundary, an effect of the non-stoichiometric boundary. It acts as a barrier for holes, while electrons hardly notice it.

Mirror twins made by the beam

The new study is one of a series of experiments by the research team on how materials change under the electron beam. In two papers in Physical Review Letters in 2012, the authors described

defect production and doping in 2D TMDs under electron irradiation[21] and measured the electron-beam-induced displacement cross sections of single-layer graphene[27]. A year later they revealed the pristine atomic structure of a MoS_2 monolayer protected from radiation damage by graphene[28].

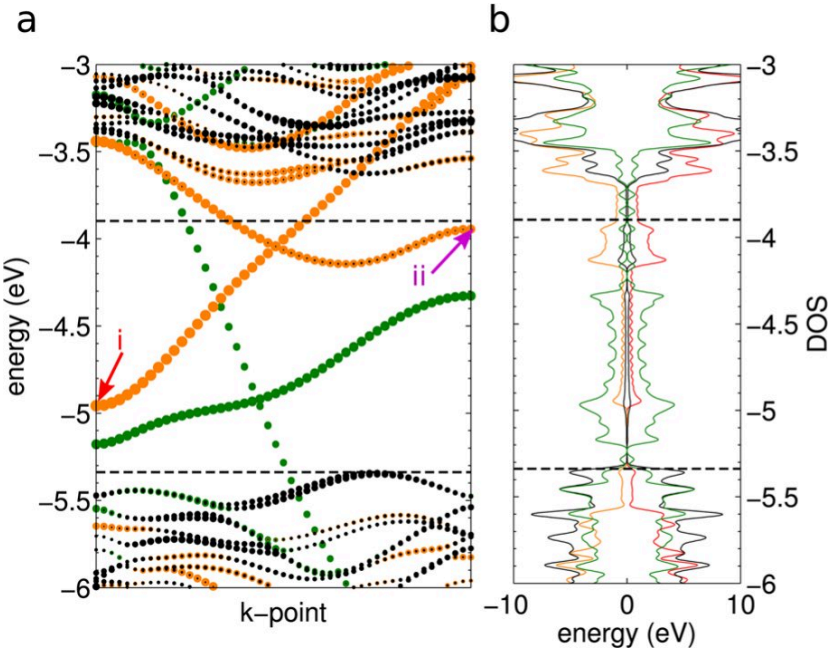

Fig. 3: Two boundary bands cross the gap.

At 80 keV, the beam knocked out single and double selenium vacancies (Fig. 6a–c). Because selenium is heavy, this is not direct knock-on damage, in which an electron of the beam simply pushes an atom out of the lattice; it must come from electronic excitations such as ionization, radiolysis or chemical etching by the beam. From the rate at which vacancies appeared and the electron dose rate, the team derived a vacancy production cross section of 3.9 barn, comparable to the 4.5 barn obtained earlier for free-standing MoS_2 at 80 keV[28].

Under continued irradiation the vacancies migrated and lined up (Fig. 6d, e), the line turned (Fig. 6f), and then, in a single frame, the atoms inside a triangular area rearranged (Fig. 6g). Afterwards a small mirror twin domain had appeared, together with an edge dislocation, and most of the vacancies were gone (Fig. 6h–j). The beam thus produced, before the eyes of the researchers, exactly the structure that the calculations predict for a selenium deficit. Another area shows the same process over one minute at a dose rate of 3.7×10^6 $e^-/(nm^2\ s)$ (Video 1): more and more vacancies form, migrate into lines and then into several small mirror domains, which grow while their boundaries move; the large domain at the lower left was there from the start and probably formed during growth. The dislocation is necessary here: the extra molybdenum for the MTB has to come from the surrounding lattice, which is pulled towards the new domain. Domains made by the beam are small and surrounded by disorder, unlike the long, regular MTBs that were present from the start of imaging, which supports that those formed during growth.

From sheet to wire

With even more selenium removed, the layer gave up being two-dimensional. Neighbouring holes grew until only narrow bridges remained, and these organized themselves into nanowires of composition MoSe (Fig. 7), as had been observed earlier in MoS_2[29]. Junhao Lin and co-workers had already sculpted MoSe wires in 2014 with the focused probe of a STEM[30]; here they formed under the broad beam of an HRTEM as selenium was lost. DFT calculations and HRTEM image simulations confirmed the structure of the wires; the model and the simulated image are shown in Fig. 8a. In the phase diagram of 2D $MoSe_2$, this marks the crossing of the boundary between two and one dimension on the selenium-poor side.

How well the images and the calculations agree, and how $MoSe_2$ compares with MoS_2 and with what random grain growth would give, is summarized in Table 1 in the box below.

The nanowires were also seen with a second kind of microscope: the box below compares Nion UltraSTEM at 60 kV vs. FEI Titan at 80 kV, that is, the 80 kV HRTEM images of this study with 60 kV STEM images taken a year later in the USA, side by side in Fig. 8 and Table 2.

Challenges named by the authors

The authors are frank about what their method cannot yet do. Growth itself cannot be watched at the atomic scale, so the origin of the mirror twins has to be read from the finished structures. The test with closed loops of mirror twin boundaries works only where such loops exist, and many boundaries do not close. The composition of $MoSe_{1.983}$ holds only for the inside of the grains: the tilt grain boundaries can be rich in either molybdenum or selenium and were not counted.

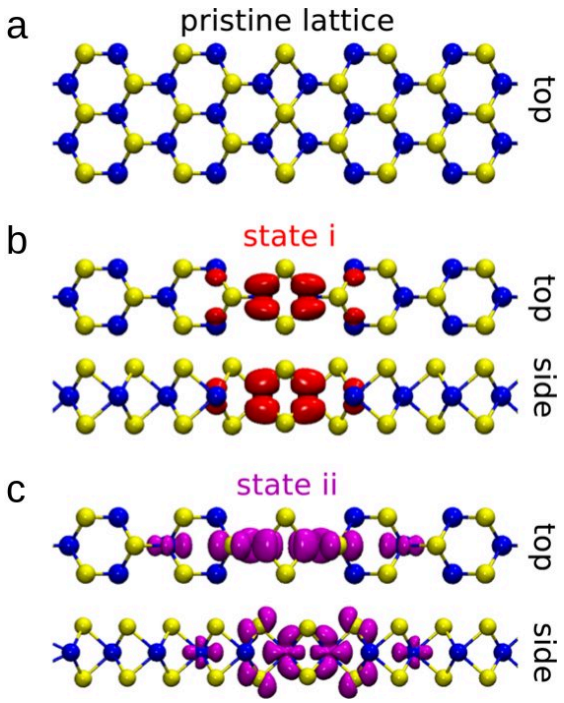

Fig. 4: Charge density of the two MTB states.

The microscope also interferes with what it measures. The electron beam creates selenium vacancies during imaging, so these had to be excluded from the composition, and how fast it does so depends on beam intensity, vacuum quality and sample preparation; for MoS_2 at 80 keV even the complete absence of beam damage has been reported. Contamination on the layer hides the lattice, which the team overcame with the special focus described above, or alternatively with a Fourier filter after recording. An earlier study of $MoSe_2$ grown on graphene had interpreted its boundaries differently, but its images were taken without aberration correction and cannot settle the atomic structure, and even residual astigmatism makes the lattice look slightly different on the two sides of a boundary.

For applications, two challenges remain. The extra electronic states along the boundaries did not improve the conductance in electrical measurements on the samples, either because electrons are scattered at the turns of the boundaries or because the many tilt grain boundaries dominate transport. And above all, the formation of mirror twin boundaries cannot yet be controlled. Further work is needed to grow them inside larger crystals and to set the growth conditions precisely enough to produce layers with a predetermined composition and domain size.

“What we’ve shown here is how the atomic scale microstructure of the binary 2D TMDs can be manipulated by the means of varying the exact composition,” said Ute Kaiser, head of the Electron Microscopy Group of Materials Science at Ulm University. Drawing a parallel to the long tradition of materials science of bulk solids, control over the composition would open up vast possibilities for engineering the properties of this new class of 2D systems.

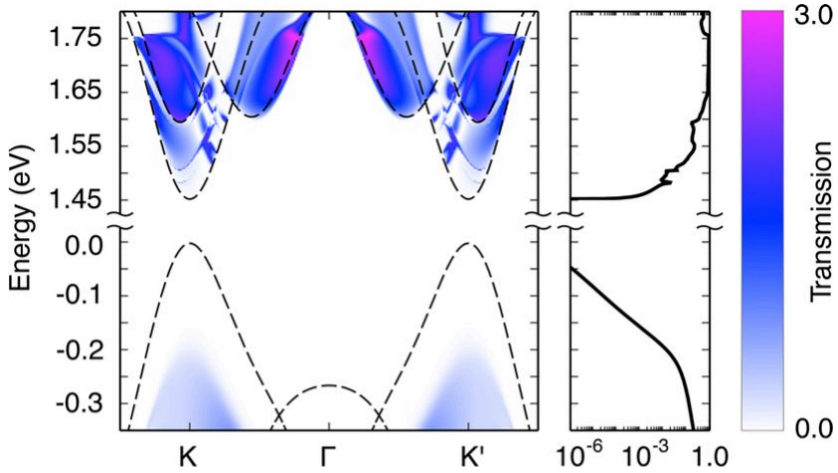

Fig. 5: Holes are blocked at the MTB.

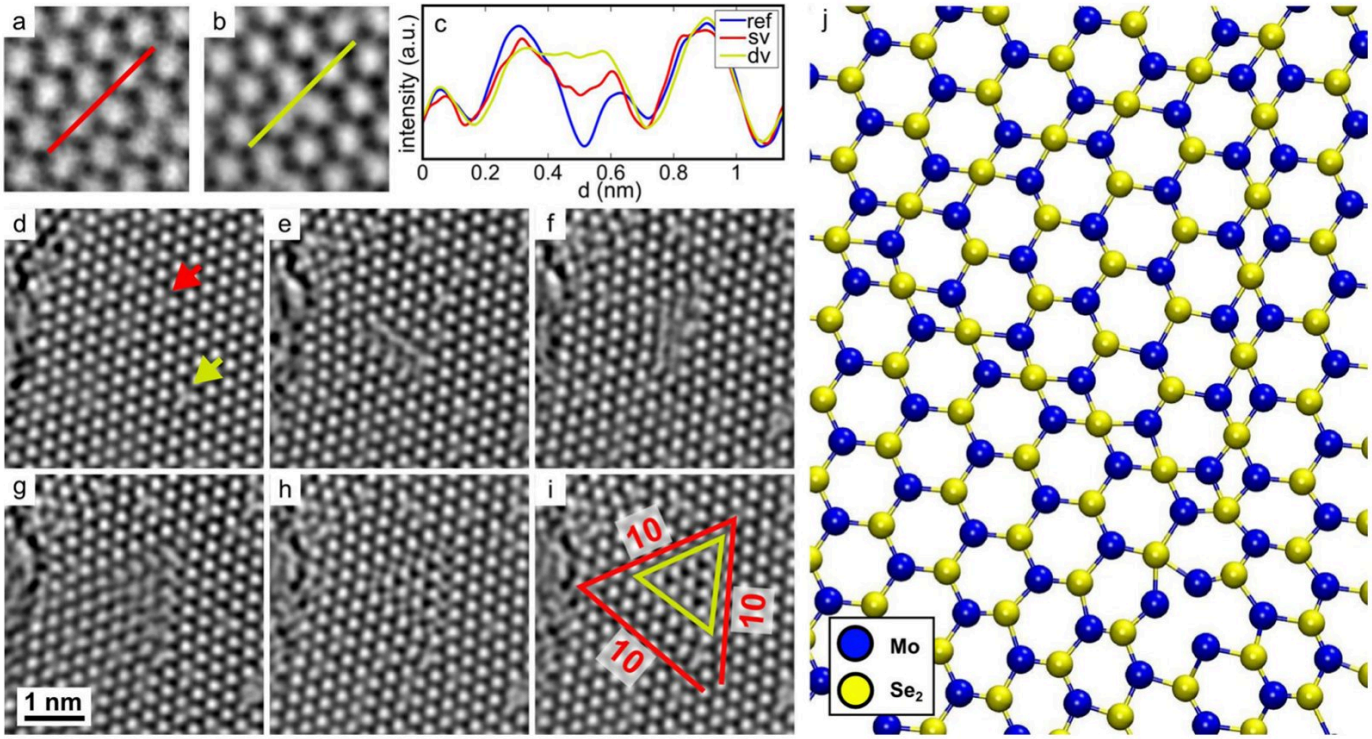

Fig. 6: Vacancies turn into a mirror twin domain.

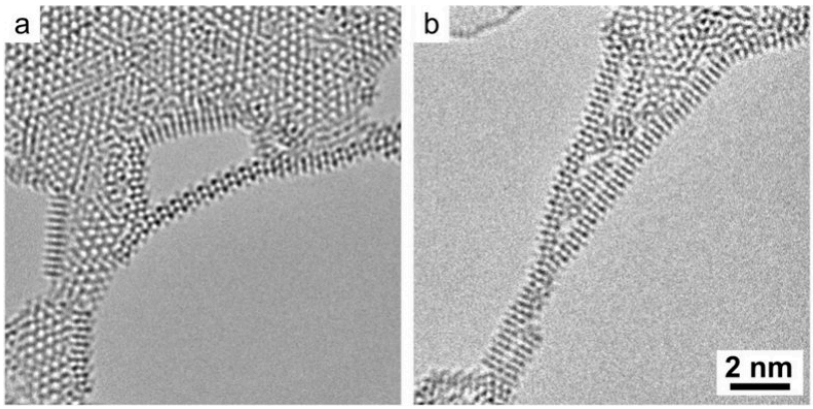

Fig. 7: MoSe nanowires between holes.

Validation: AC-HRTEM at 80 kV vs. DFT calculations

The study rests on two independent methods: images from the C_s-corrected FEI Titan at 80 kV in Ulm, and density functional theory calculations of energies, electronic structure and transport at Aalto University and EPFL. Table 1 sets each observation against the prediction or the earlier measurement it was checked with. Six of eight checks agree. The two that do not are just as telling: the mirror twins are far too frequent to come from merging grains, and the extra conduction channels along the boundaries do not show up in a real, polycrystalline layer.

	Observed (AC-HRTEM, 80 kV)	Prediction or comparison	Agreement
Structure of the mirror twin boundary	only one type, structure (1) (Fig. 1c, d)	DFT: structure (1) is the lowest of six candidates, by 0.3 eV (Fig. 2a)	yes
Growth direction of the grains	no boundaries where Mo edges meet: grains grew along their Se edges	DFT: the leading Se edge is the most stable edge under Mo-rich conditions	yes
How often mirror twins occur	0.093 nm/nm^2 MTB vs. 0.097 nm/nm^2 tilt boundary, about 1 : 1	grains merging at random angles: one boundary in six	no: MTBs form during growth
Form of the Se deficit in the grown layer	dense MTBs, no vacancy lines	DFT: vacancy lines cost far more energy than MTBs, unlike in MoS_2 (Fig. 2b)	yes
Removing Se with the beam	vacancies line up and turn into a mirror twin domain (Fig. 6)	DFT: MTB-rich layers lie below a $MoSe_2$/Mo_3Se_4 mixture (Fig. 2c)	yes
Vacancy production cross section	3.9(4) barn for $MoSe_2$	4.5(4) barn for free-standing MoS_2 at 80 keV [28]	comparable
MoSe nanowires at high Se loss	wires bridging holes (Fig. 7a, b)	DFT-relaxed model and simulated HRTEM image (Fig. 7c–e); the same wire type in 60 kV STEM a year later (Fig. 8) [31]	yes
Conductance along the boundaries	electrical measurements on the samples: no improvement	DFT: states in the gap could raise the conductance along straight MTBs (Figs. 3, 4)	no: scattering at turns and tilt boundaries

Table 1: What the AC-HRTEM images at 80 kV show compared with the DFT calculations, with free-standing MoS_2 and with random grain growth (numbers from the paper; in brackets the uncertainty of the last digit).

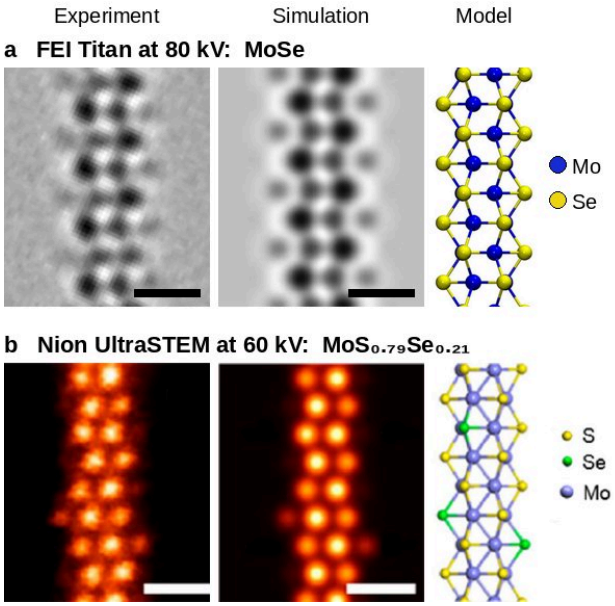

Fig. 8: MoSe wire in HRTEM and STEM.

Validation: Nion UltraSTEM at 60 kV vs. FEI Titan at 80 kV

In 2016, Junhao Lin, Yuyang Zhang, Wu Zhou and Sokrates Pantelides of Vanderbilt University and Oak Ridge National Laboratory checked the MoSe nanowires independently and cited the present study[31]. Their microscope works differently: instead of illuminating the sample with a broad parallel beam, an aberration-corrected Nion UltraSTEM 100 (today Bruker) scans a focused probe across it at 60 kV (Fig. 8; 100 kV only in their voltage test, see below) and records the electrons scattered to high angles (Z-contrast). Atoms then appear bright, and the brightness of each atomic column grows with its atomic number, so selenium can be told apart from sulfur. Table 2 compares the two set-ups.

	FEI Titan at 80 kV (this study)	Nion UltraSTEM at 60 kV (Lin et al. 2016)
Where	Ulm University	Oak Ridge National Laboratory, USA
Microscope	FEI Titan 80-300 (today Thermo Fisher Scientific), TEM	Nion UltraSTEM 100 (today Bruker), scanning TEM (STEM)
Corrector	CEOS, C_s of the imaging lens	C_s of the probe-forming lens
Voltage	80 kV	60 kV (100 kV only in the voltage test)
Beam	broad parallel beam	focused probe (31 mrad) scanned across the sample
Image formation	phase contrast (HRTEM); at negative defocus the atoms appear dark	Z-contrast (annular dark field, 86–200 mrad); atoms bright, brighter with atomic number
Starting material	MBE-grown $MoSe_2$ monolayer	$MoSe_2$ monolayer, $MoS_2/MoSe_2$ bilayer, alloyed monolayers
Nanowires	MoSe, formed between holes under prolonged irradiation	MoSe, MoS_xSe_{1-x}, $Mo_xW_{1-x}S$, sculpted where the probe scans
What it shows	wire structure, confirmed by DFT model and HRTEM simulation (Fig. 8a)	wire structure and the position of each Se atom from column intensities (Fig. 8b)

Table 2: The two aberration-corrected microscopes that imaged the MoSe nanowires (STEM data from Lin et al. [31]).

Both microscopes show the same kind of wire (Fig. 8). In the Titan, the MoSe wire appears as a chain of dark atom columns, matched by the HRTEM image simulation and the DFT model of this study. In the STEM, a wire with the same backbone of molybdenum atoms capped by chalcogen atoms appears as bright columns, and its simulated image reproduces the intensity of each column. With the focused probe, Lin and co-workers could also choose where a wire forms, and they found that MoSe wires can twist, kink, branch and join in junctions while staying metallic.

The STEM study also sharpens the picture of how the beam acts on the chalcogen atoms. Starting from a stacked $MoS_2/MoSe_2$ bilayer with as much selenium as sulfur, a wire sculpted at 60 kV lost its selenium within less than a minute: its Se content fell from 33 % after half a second to 17 % after 23.5 s and 6 % after 43.5 s, and the wires ended as MoS. At 100 kV they ended as MoSe. In the wire, sulfur is knocked out only above about 88 kV and selenium above about 180 kV, while the Mo–S bond (5.33 eV) is stronger than the Mo–Se bond (4.91 eV). At 60 kV the stronger Mo–S bonds therefore win; at 100 kV sulfur no longer survives. Like this study, where selenium was lost at 80 kV far below its knock-on threshold, it shows that the beam can change the chalcogen content of these materials in a controlled way.

Resource

Lehtinen, O., Komsa, H.-P., Pulkin, A., Whitwick, M. B., Chen, M.-W., Lehnert, T., Mohn, M. J., Yazyev, O. V., Kis, A., Kaiser, U., Krasheninnikov, A. V. (2015). Atomic Scale Microstructure and Properties of Se-Deficient Two-Dimensional $MoSe_2$.

ACS Nano **9**(3), 3274–3283.

References

1. Lehtinen, O., Komsa, H. P., Pulkin, A., Whitwick, M. B., Chen, M. W., Lehnert, T., Mohn, M. J., Yazyev, O. V., Kis, A., Kaiser, U. A., & Krasheninnikov, A. V. (2015). Atomic Scale Microstructure and Properties of Se-Deficient Two-Dimensional $MoSe_2$. ACS Nano, 9: 3274-3283. https://doi.org/10.1021/acsnano.5b00410
2. Callister, W. D., & Rethwisch, D. G. (2007). Materials Science and Engineering: An Introduction, 7th ed., pp. 665-715. New York: Wiley.
3. Jariwala, D., Sangwan, V. K., Lauhon, L. J., Marks, T. J., & Hersam, M. C. (2014). Emerging device applications for semiconducting two-dimensional transition metal dichalcogenides. ACS Nano, 8: 1102-1120. https://doi.org/10.1021/nn500064s
4. Kim, K. K., Hsu, A., Jia, X., Kim, S. M., Shi, Y., Hofmann, M., Nezich, D., Rodriguez-Nieva, J. F., Dresselhaus, M., Palacios, T., & Kong, J. (2011). Synthesis of monolayer hexagonal boron nitride on Cu foil using chemical vapor deposition. Nano Letters, 12: 161-166. https://doi.org/10.1021/nl203249a
5. Shi, Y., Zhou, W., Lu, A. Y., Fang, W., Lee, Y. H., Hsu, A. L., Kim, S. M., Kim, K. K., Yang, H. Y., Li, L.-J., Idrobo, J.-C., & Kong, J. (2012). Van der Waals epitaxy of MoS_2 layers using graphene as growth templates. Nano Letters, 12: 2784-2791. https://doi.org/10.1021/nl204562j
6. Najmaei, S., Liu, Z., Zhou, W., Zou, X., Shi, G., Lei, S., Yakobson, B. I., Idrobo, J.-C., Ajayan, P. M., & Lou, J. (2013). Vapour phase growth and grain boundary structure of molybdenum disulphide atomic layers. Nature Materials, 12: 754-759. https://doi.org/10.1038/nmat3673
7. Kutana, A., Penev, E. S., & Yakobson, B. I. (2014). Engineering electronic properties of layered transition-metal dichalcogenide compounds through alloying. Nanoscale, 6: 5820-5825. https://doi.org/10.1039/C4NR00177J
8. Mann, J., Ma, Q., Odenthal, P. M., Isarraraz, M., Le, D., Preciado, E., Barroso, D., Yamaguchi, K., von Son Palacio, G., Nguyen, A., Tran, T., Wurch, M., Nguyen, A., Klee, V., Bobek, S., Sun, D., Heinz, T. F., Rahman, T. S., Kawakami, R., & Bartels, L. (2014). 2-Dimensional Transition Metal Dichalcogenides with Tunable Direct Band Gaps: MoS_2(1–x)Se2x Monolayers. Advanced Materials, 26: 1399-1404. https://doi.org/10.1002/adma.201304389
9. Li, H., Duan, X., Wu, X., Zhuang, X., Zhou, H., Zhang, Q., Zhu, X., Hu, W., Ren, P., Guo, P., Ma, L., Fan, X., Wang, X., Xu, J., Pan, A., & Duan, X. (2014). Growth of Alloy MoS2xSe2(1–x) Nanosheets with Fully Tunable Chemical Compositions and Optical Properties. Journal of the American Chemical Society, 136: 3756-3759. https://doi.org/10.1021/ja500069b
10. Chen, Y., Xi, J., Dumcenco, D. O., Liu, Z., Suenaga, K., Wang, D., Shuai, Z., Huang, Y.-S., & Xie, L. (2013). Tunable band gap photoluminescence from atomically thin transition-metal dichalcogenide alloys. ACS Nano, 7: 4610-4616. https://doi.org/10.1021/nn401420h
11. Cheng, Y., Guo, Z. B., Mi, W. B., Schwingenschlögl, U., & Zhu, Z. (2013). Prediction of two-dimensional diluted magnetic semiconductors: Doped monolayer MoS_2 systems. Physical Review B, 87: 100401. https://doi.org/10.1103/PhysRevB.87.100401
12. McDonnell, S., Addou, R., Buie, C., Wallace, R. M., & Hinkle, C. L. (2014). Defect-dominated doping and contact resistance in MoS_2. ACS Nano, 8: 2880-2888. https://doi.org/10.1021/nn500044q
13. Kim, I. S., Sangwan, V. K., Jariwala, D., Wood, J. D., Park, S., Chen, K. S., Shi, F., Ruiz-Zepeda, F., Ponce, A., Jose-Yacaman, M., Dravid, V. P., Marks, T. J., Hersam, M. C., & Lauhon, L. J. (2014). Influence of stoichiometry on the optical and electrical properties of chemical vapor deposition derived MoS_2. ACS Nano, 8: 10551-10558. https://doi.org/10.1021/nn503988x
14. Conan, A., Goureaux, G., & Zoaeter, M. (1975). Transport properties of $MoTe_{2-x}$ and $MoSe_{2-x}$ compounds between 130 and 300 K. Journal of Physics and Chemistry of Solids, 36: 315-320. https://doi.org/10.1016/0022-3697(75)90029-3
15. Spiesser, M., Marchal, C., & Rouxel, J. (1968). Sur Des Phases Molybdene-Selenium Non Stoechiometriques. Compt. Rend. Acad. Sci., 266: 1583-1586.
16. Wang, Q. H., Kalantar-Zadeh, K., Kis, A., Coleman, J. N., & Strano, M. S. (2012). Electronics and optoelectronics of two-dimensional transition metal dichalcogenides. Nature Nanotechnology, 7: 699-712. https://doi.org/10.1038/nnano.2012.193
17. Grantab, R., Shenoy, V. B., & Ruoff, R. S. (2010). Anomalous strength characteristics of tilt grain boundaries in graphene. Science, 330: 946-948. https://doi.org/10.1126/science.1196893
18. Yazyev, O. V., & Louie, S. G. (2010). Topological defects in graphene: Dislocations and grain boundaries. Physical Review B, 81: 195420. https://doi.org/10.1103/PhysRevB.81.195420
19. Mori, T., Abe, H., Saiki, K., & Koma, A. (1993). Characterization of epitaxial films of layered materials using Moiré images of scanning tunneling microscope. Japanese Journal of Applied Physics, 32: 2945. https://doi.org/10.1143/JJAP.32.2945
20. Murata, H., & Koma, A. (1999). Modulated STM images of ultrathin $MoSe_2$ films grown on MoS_2 (0001) studied by STM/STS. Physical Review B, 59: 10327. https://doi.org/10.1103/PhysRevB.59.10327
21. Komsa, H. P., Kotakoski, J., Kurasch, S., Lehtinen, O., Kaiser, U., & Krasheninnikov, A. V. (2012). Two-dimensional transition metal dichalcogenides under electron irradiation: defect production and doping. Physical Review Letters, 109: 035503. https://doi.org/10.1103/PhysRevLett.109.035503
22. Komsa, H. P., Kurasch, S., Lehtinen, O., Kaiser, U., & Krasheninnikov, A. V. (2013). From point to extended defects in two-dimensional MoS_2: evolution of atomic structure under electron irradiation. Physical Review B, 88: 035301. https://doi.org/10.1103/PhysRevB.88.035301
23. Hanna, G., Mattheis, J., Laptev, V., Yamamoto, Y., Rau, U., & Schock, H. W. (2003). Influence of the selenium flux on the growth of Cu(In,Ga)Se_2 thin films. Thin Solid Films, 431: 31-36. https://doi.org/10.1016/S0040-6090(03)00242-6
24. Kresse, G., & Furthmüller, J. (1996). Efficient iterative schemes for ab initio total-energy calculations using a plane-wave basis set. Physical Review B, 54: 11169. https://doi.org/10.1103/PhysRevB.54.11169
25. Perdew, J. P., Burke, K., & Ernzerhof, M. (1996). Generalized gradient approximation made simple. Physical Review Letters, 77: 3865. https://doi.org/10.1103/PhysRevLett.77.3865
26. Tison, Y., Lagoute, J., Repain, V., Chacon, C., Girard, Y., Joucken, F., Sporken, R., Gargiulo, F., Yazyev, O. V., & Rousset, S. (2014). Grain Boundaries in Graphene on SiC $(000\bar{1})$ Substrate. Nano Letters, 14: 6382-6386. https://doi.org/10.1021/nl502854w
27. Meyer, J. C., Eder, F., Kurasch, S., Skakalova, V., Kotakoski, J., Park, H. J., Roth, S., Chuvilin, A., Eyhusen, S., Benner, G., Krasheninnikov, A. V., & Kaiser, U. (2012). Accurate measurement of electron beam induced displacement cross sections for single-layer graphene. Physical Review Letters, 108: 196102. https://doi.org/10.1103/PhysRevLett.108.196102
28. Algara-Siller, G., Kurasch, S., Sedighi, M., Lehtinen, O., & Kaiser, U. (2013). The pristine atomic structure of MoS_2 monolayer protected from electron radiation damage by graphene. Applied Physics Letters, 103: 203107. https://doi.org/10.1063/1.4830036
29. Liu, X., Xu, T., Wu, X., Zhang, Z., Yu, J., Qiu, H., Hong, J.-H., Jin, C.-H., Wang, X.-R., Sun, L.-T., & Guo, W. (2013). Top–down fabrication of sub-nanometre semiconducting nanoribbons derived from molybdenum disulfide sheets. Nature Communications, 4: 1776. https://doi.org/10.1038/ncomms2803
30. Lin, J., Cretu, O., Zhou, W., Suenaga, K., Prasai, D., Bolotin, K. I., et al. (2014). Flexible metallic nanowires with self-adaptive contacts to semiconducting transition-metal dichalcogenide monolayers. *Nature Nanotechnology*, **9**, 436-442. https://doi.org/10.1038/nnano.2014.81
31. Lin, J., Zhang, Y., Zhou, W., & Pantelides, S. T. (2016). Structural Flexibility and Alloying in Ultrathin Transition-Metal Chalcogenide Nanowires. *ACS Nano*, **10**, 2782-2790. https://doi.org/10.1021/acsnano.5b07888